Journal of Petroleum Science and Technology 13(1): 37, 2023, Pages 27-40
DOI:10.22078/jpst.2023.5116.1878

Journal of Petroleum Science and Technology
Research Paper
https://jpst.ripi.ir/

Rapid and Efficient Demulsification of W/O Emulsions of Crude Oil by Nanocomposites based on Titanium Dioxide with Carbonaceous Substrates

Tania Bigdeli, Marzieh Shekarriz*, Ali Mehdizadeh and Amir Nasser Ahmadi
Chemical, Polymeric, and Petrochemical Technology Research Division, Faculty of Research and Development in Downstream Petroleum Industry, Research Institute of Petroleum Industry (RIPI), Tehran, Iran

Abstract
TiO_2 nanocomposites on carbonaceous compounds, such as carboxyl-functionalized, multi-walled carbon nanotubes (MWCNT-COOH), and graphene oxide (GO) were synthesized by the sol-gel method. The samples were coded as TiO_2 (*T*), TiO_2-MWCNT-COOH (*TM*), and TiO_2-GO (*TG*). The effect of the addition of carbonaceous compounds on the enhancement of demulsification efficiency of TiO_2 nanocomposites in crude oil (W/O) emulsions was then investigated. FT-IR, Raman, and morphological analyses such as FE-SEM, EDXS, XRD, HR-TEM, DRS, BET surface area, and TGA were used to determine the properties and structures of the nanoparticles prepared. In addition, the demulsification efficiency of three nanoparticles was studied under various concentrations, settling times, and temperature conditions by bottle test. According to the screening results, TG was selected as the best sample. The response surface method with a central composite design (CCD) was used to optimize the demulsification activity of TiO_2 nanocomposites with graphene oxide (TG). Thus, the impacts of temperature, demulsifier concentration, and time were studied by the RSM-CCD method. Ultimately, the results indicated ~100% demulsification efficiency under optimal conditions at concentration, temperature, and time of 75 ppm, 65°C, and 120 min., respectively.

Keywords: TiO_2, Carbonaceous Substrates, Sol-gel, Demulsification, Statistical methodology.

Introduction
During many steps of crude oil extraction and processing, stable W/O emulsions are formed [1-2]. The presence of asphaltenes and resins as natural emulsifiers, along with wax and solids, mostly forms these emulsions [3]. Rigid films can form at the oil/water interface when all these components are organized. Emulsion stability is affected by numerous factors, including pH, temperature, water droplet size, viscosity, oil-to-brine ratio, surface tension, and the differences between the phase densities [4-7]. Water in oil causes serious problems in the petroleum industry, such as catalyst poisoning, corrosion, fouling, increased pressure drop, and transportation costs. Therefore, it is necessary to break emulsions and separate water from crude oil [8-10]. Various water removal methods have been reported to overcome the drawbacks associated with emulsion stability. It is required to break the oil/water interface to separate water from crude oil completely. This is often known as de-salting and de-watering and may be performed by chemical, mechanical, thermal, and electrostatic approaches or combinations thereof. Chemical methods are the most conventional demulsification methods. The combination of thermal and chemical methods can effectively break an interfacial film. As an alternative method, nanotechnology can improve water separation. In addition, nano metal oxides can be employed as efficient demulsifiers [11-13].
For example, Fan Ye *et al*. reported a light transmittance of up to 79.1% using RGO/TiO_2 at a concentration and settling time of 500 mg/L and 30 min., respectively, at ambient temperature in 2019 [14]. In the same year, Hassan showed that silica nanoparticles with a diameter of 25 nm at 60 ppm concentration and a 0.5:1 ratio of silica nanosuspension to chemical demulsifier increased water separation by 53% [15-16]. Haiyan Xu reported magnetic, multi-walled carbon nanotubes (M-MWCNTs) suitable for acidic to alkaline conditions of crude O/W emulsions by tuning the number of surface functional groups such as –OH, –NH_2, and –COOH in 2019. M-MWCNTs were reportedly efficient demulsifiers with maximum demulsification efficiency at a 400 mg/L concentration. Water separation from crude oil W/O emulsions was enhanced by the synergistic interaction

**Corresponding author:* Marzieh Shekarriz, Chemical, Polymeric, and Petrochemical Technology Research Division, Faculty of Research and Development in Downstream Petroleum Industry Research Institute of Petroleum Industry (RIPI), Tehran, Iran
E-mail addresses: shekarriz@ripi.ir
Received 2023-05-01, Received in revised form 2023-09-26, Accepted 2023-10-17, Available online .....

of π-π or n-π types or both aromatics/functional groups of asphaltenes and MWCNTs. The major demulsification mechanism in neutral media was the interfacial adsorption of π-π or n-π interactions or both [17]. In 2020, Kin Kit Fung used polyethyleneimine (PEI) to prepare a stable hydrogel composite. Afterward, the conditions for immobilizing graphene oxide (GO) on PEI-modified κ-Carrageenan (κC) beads were suitably optimized. An immobilization yield of 77% was obtained using 2% PEI, activation time of 2 h, and pH of 6.5 with a 70% average demulsification efficiency [18]. A literature survey in this area indicates that TiO_2 is one of the most conventional and safe metal oxides. Not only can TiO_2 break oil in water emulsions, but it can also efficiently degrade organic pollutants [15-18]. In 2014, Nikkhah *et al*. prepared different TiO_2 nanoparticles and reported better demulsification efficiency of TiO_2 and demulsifier mixtures compared with the single demulsifier [19]. Nanocrystalline TiO_2 can be used effectively in various applications, including solar power conversion, gas sensing, photocatalysis, adsorbents, and optical filters. Despite various applications of nano TiO_2, such as those in food, sports, cosmetics, medicine, electronics, and aerospace industries, the feasibility of applying this crystalline particle in the demulsification of W/O emulsions has not yet been investigated. Therefore, a high-performance compound can be obtained by modification of the TiO_2 structure. Using elements such as Ag, Sb, etc., to improve the TiO_2 activity and chemical substrates such as carbonaceous nanomaterials can help expand the surface, reduce consumption, and enhance its favorable physical properties. The effect of TiO_2 nanohybrid on water separation was studied in this work to enhance the demulsification efficiency. In this regard, nano TiO_2 particles were synthesized by sol-gel technique, which allows the preparation of highly pure compounds, ensuring delicately adjusted physicochemical characteristics through reasonable parameter selection and, therefore, the synthesis method. Due to the exceptional characteristics of this method, it may be applied in the commercial production of high-quality nanoparticles [20-23]. Statistical modeling is the best option to optimize laboratory conditions. Design of experiment (DOE) is used as a collection of valuable mathematical techniques for the systematic analysis and statistical modeling in which input variables or factors are used to optimize the desirable responses [24]. In our previous work, the demulsification activity of chitosan with titanium dioxide nanohybrid on graphene oxide (CT/TZG) was optimized *via* the response surface method with a central composite design (CCD). The results revealed a maximum demulsification efficiency of ~100 % [25]. The principal purpose of this work is to develop a new method to overcome the drawbacks of W/O emulsions using unprecedented aspects of nanotechnology. The work is aimed at achieving a TiO_2 nanoparticle-based, highly active demulsifier. In addition, a trace quantity of Zr dopant has been applied in TiO_2 lattices to improve their efficiency. Small MWCNT-COOH and GO amounts have also been added to increase the specific area and thermal stability of TiO_2. The statistical methodology has been used to optimize the demulsification conditions using DOE (Minitab 20 software). The demulsifier efficiency has been investigated by bottle test.

Materials and Methods

Titanium tetraisopropoxide (TTIP, 97%) was obtained from Panreac Co. (Spain). Functionalized multi-walled carbon nanotubes (MWCNT–COOH, > 95%, OD: 20-30 nm) and graphene oxide nanoplatelets (GONPs, > 99.5%, 2-18 nm with 32 layers) were supplied by the US research nanomaterials, Inc. The rest of the chemicals, including hydroxypropyl cellulose (HPC), cetyltrimethylammonium bromide (CTAB), nitric acid (65%), absolute ethanol (99%), and all solvents were obtained from Merck Chemical Co. (Germany). The crude oil from the Asmari reservoir of Ahvaz oilfield (Iran) was used as the oil phase for W/O emulsions.

The SARA test was performed using a chromatography column. An Anton Paar (SVM 3000) viscometer was used to measure viscosity and density. FT-IR spectra were recorded using KBr pellets in the 400-4000 cm^{-1} wavenumber range on a Thermo Nicolet Nexus 870 FTIR spectrophotometer. The phase characterization of Ti-NPs was performed by XRD using a SCIFERT-3003 PTS instrument with CuK_α radiation in the 0-100 (2θ) range at ambient temperature. FE-SEM (HITACHI S-4160) was used to investigate the microanalysis and morphology of Ti-NPs. The specific surface area of Ti-NP was determined by BET measurement (Quanta chrome Nova 2200). The nanostructure of the samples was investigated by HR-TEM (Philips EM 208 electron microscope). The EDXS analysis was performed using a HITACHI S-4160 instrument. Diffuse reflection/transmittance spectroscopy (DRS/DTS) was performed using an Avantes spectrophotometer (Avaspec-2048-TEC) with an AvaLamp DH-S setup. Thermogravimetric analysis (TGA) was carried out using a Mettler TGA-SDTA851 analyzer. Crude oil and water were mixed using A MICCRA D-1 (30349) homogenizer.

Preparation of Ti-NPs.

TiO_2 NPs were prepared by the sol-gel method. TTIP (5 ml) was first dissolved in absolute ethanol (70 ml) (75:1 molar ratio), followed by stirring for 15 min. Afterward, HPC (0.1 g) was added as a cross-linking agent and stabilizer to form a precursor solution, and the resulting mixture was stirred continuously for 15 min. to yield a yellow transparent sol (Sol 1). A mixture of absolute ethanol (22 ml), CTAB (0.1 g), and nitric acid (280 µl) (Sol 2) with molar ratios of 0.47, 0.00028, and 0.0044, respectively, was next added dropwise for 30 min. into Sol 1 by fast stirring to form a transparent sol. Afterward, a homogenizer (20000 rpm rotation speed) was used to disperse the two sols better. This sol (Sol 1 + Sol 2) was aged at ambient temperature for 48 h to yield a gel, which was kept for some time before drying to strengthen the bonds between the particles. The gel was then spontaneously air-dried. The solvents were removed by heating for 30 min. at 100°C, then calcination at 525°C in an electric furnace for 4 h. The same methods were used to prepare TiO_2/MWCNT-COOH (TM) and TiO_2/GO NPs (TG) . Nevertheless, in this stage, Sol 2 was added to MWCNT-COOH (0.02 g) and GO (0.01 g), and the process was repeated [26].

Characterization of Crude oil

The Asmari light crude oil from the Ahvaz oilfield (Iran) was used in this study. Table 1 shows the physical and chemical properties and the results of the corresponding SARA test.

Table 1 Chemical and physical characterization and the SARA test of Crude Oil.

Physical characterization		
Type of characterization	Value	Standard Test Method
API gravity at 15°C	31.63	ASTM D-1298
Kinematic viscosity @15ºC, cSt	16.71	ASTM D-7042
Density @15°C, g/ml	0.8674	ASTM D-4052
SARA Fractionation Test		
Above 200ºC		
Saturates, wt. %	71.8	ASTM D-6560
Aromatics, wt. %	20.4	
Resins, wt. %	7.8	
Asphaltenes, wt. %	< 0.5	
Including volatiles at 200ºC		
Saturates, wt. %	63.8	ASTM D-6560
Aromatics, wt. %	18.1	
Resins, wt. %	6.9	
Asphaltenes, wt. %	< 0.5	

Statistical Methodology

A full factorial design was carried out to investigate the impact of the variables on the interfacial tension and the interactions among them. The regression analysis of the experimental data and plotting of the response surface (three factors each in two blocks) were performed using the Minitab (ver. 20) statistical software package. The statistical parameters were also estimated using the ANOVA method. According to the previous results, the demulsifier dosage, time, and temperature were chosen as the major parameters [24]. Sufficient choices of responses, levels, and factors are required by experimental design. The mathematical model was fitted to the data, and the Analysis of Variance (ANOVA) was performed to find the significance of the model. The optimum demulsification conditions were determined by CCD using the modified TiO_2 nanohybrid.

Demulsification Activity of Ti-NPs

Bottle Test Procedure

First, crude oil (85 ml) and freshwater (15 ml) were completely mixed by a homogenizer (35000 rpm and 30 min.). Then, the emulsions were poured into standard, graduated, 100 mL DURAN 50 (Germany) conical bottles. Different Ti-NP concentrations were added by micropipettes, after which the bottles were capped using plastic stoppers, vigorously shaken 100 times in horizontal and vertical directions, and placed inside metal baskets in sets of 12 in a thermostat water bath covering the crude oil. Eventually, the demulsification efficiency (DE) was determined by the water removal percentage using the following equation [27]:

$$DE\ (\%) = [\frac{V}{V_0}] * 100\% \quad (1)$$

where V and V_0 are the separated and initial water volumes, respectively.

Results and Discussion

Following a thorough literature search [14-20, 27], it was attempted to choose a new sample with satisfactory behavior. Metal oxide nanoparticles were chosen given their extraordinary properties and promising potential for various applications. The efficiency is predicted to increase by reducing particle sizes to nano dimensions. At first, different parameters affecting the Ti-NP size, such as sol concentration, homogenizer rotation speed) rpm), time of the rest of the gel, final calcination temperature, etc., were investigated (Table 2). In the second part, the carbonaceous substrates were applied in water, and petroleum treatment was selected based on the previous studies. TiO_2 was used with carbonaceous substrates to obtain a novel demulsifier with increased efficiency and higher surface area (Fig. 1). The rest time of the gel depends on the seasonal conditions, ambient temperature, and sol concentration. However, 48-72 h was enough to form the gel and organize Ti-NP particles. To achieve the most desirable TiO_2 activity, the calcination temperature of 525 ± 5ºC was applied such that the rutile phase percentage increased at high temperatures, leading to decreased TiO_2 activity. Amorphous and brookite phases were obtained at lower temperatures, and TiO_2 activity decreased again.

Table 2 Impact of sol concentration and homogenizer rotation rate on size of Ti-NPs

Sol concentration (molar ratio of TTIP to ethanol)	Ti-NPs size (nm)	Homogenizer rotation rate (rpm)	Ti-NPs size (nm)
0.5 : 75	gel not formed	5000	85
1 : 75	23	10000	62
2 : 75	30	15000	40
3 : 75 (particles agglomerate)	65	20000	26

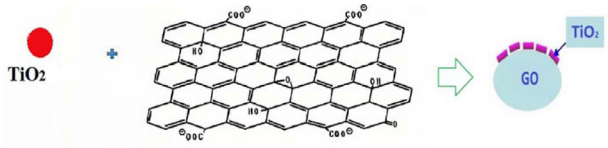

Fig. 1 Summary of preparation of Ti-NP/GO.

Thus, the calcination temperature of 525 ± 5°C was used. Several parameters affect the sol-gel process (condensation) and hydrolysis reactions, including mineral oxide activity, solution pH, solvent nature, temperature, and the additive applied [30-33]. Thus, the parameters affecting demulsification efficiency were attempted to optimize. Carbonaceous compounds such as carboxyl-functionalized, multi-walled carbon nanotubes, and graphene oxide were added to modify TiO_2 and expand its surface area. The selection of carbonaceous compound amount depended on the demulsification efficiency. Table 3 shows the results.

Table 3 BET Surface area analysis and demulsification efficiency of Ti-NPs with carbonaceous compounds.

Sample	BET (m^2/g)	*Demulsification efficiency, %
TiO_2	108	10
TiO_2/MWCNT-$COOH_{0.01}$	160	40
TiO_2/MWCNT-$COOH_{0.02}$	192	60
TiO_2/$GO_{0.01}$	205	80
TiO_2/$GO_{0.02}$	215	85

* Demulsification efficiency was determined under optimal conditions of 150 ppm, 40ºC, and 120 min.

FTIR Spectroscopy.

The FTIR spectra of Ti-NPs are shown in Fig. 2. The bending stretching vibration of O–Ti–O and Ti–O–Ti could be observed in the 530-675 cm^{-1} range. Furthermore, the peaks associated with H–O–H and Ti–O–C were observed at ~1615 and ~1200 cm^{-1}, respectively. The peaks ascribed to Ti–O and Ti–OH stretching vibration were observed in the ~890-1260 cm^{-1} range, and the C–O peak was observed at ~ 1100 cm^{-1}. The peak associated with the C=O stretching vibration of TG appeared at 1639.48 cm^{-1} [28-32].

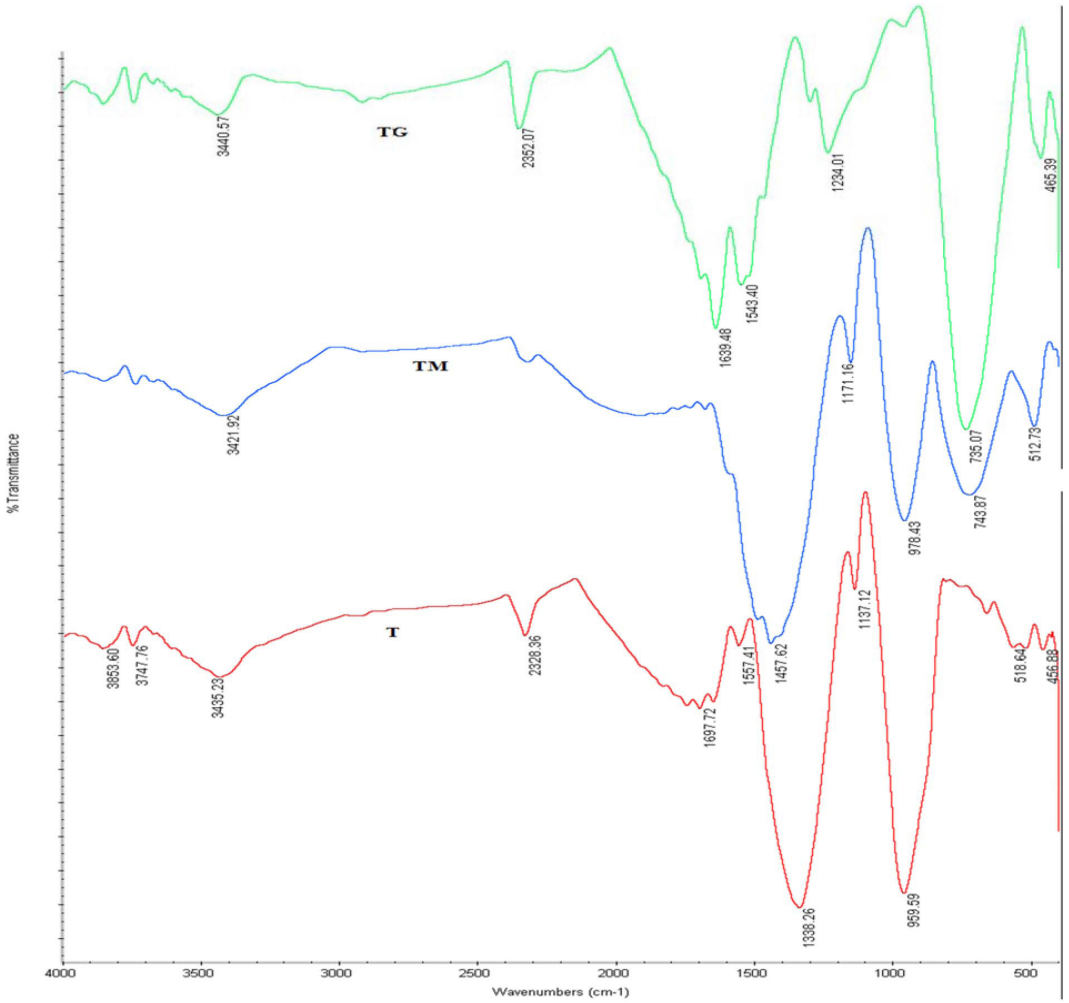

Fig. 2 FT-IR spectra of powder samples of Ti-NPs.

Raman Spectroscopy

Fig. 3 shows the Raman spectra of Ti-NPs. Carbonaceous substrates can change the vibration of TiO_2 lattices. Considering the higher activity of titanium in the anatase phase, detecting this phase is very important. According to the literature, the couriers at 144, 197, 399, 531, and ~ 639 cm^{-1} are related to the anatase allotropes [32-35].

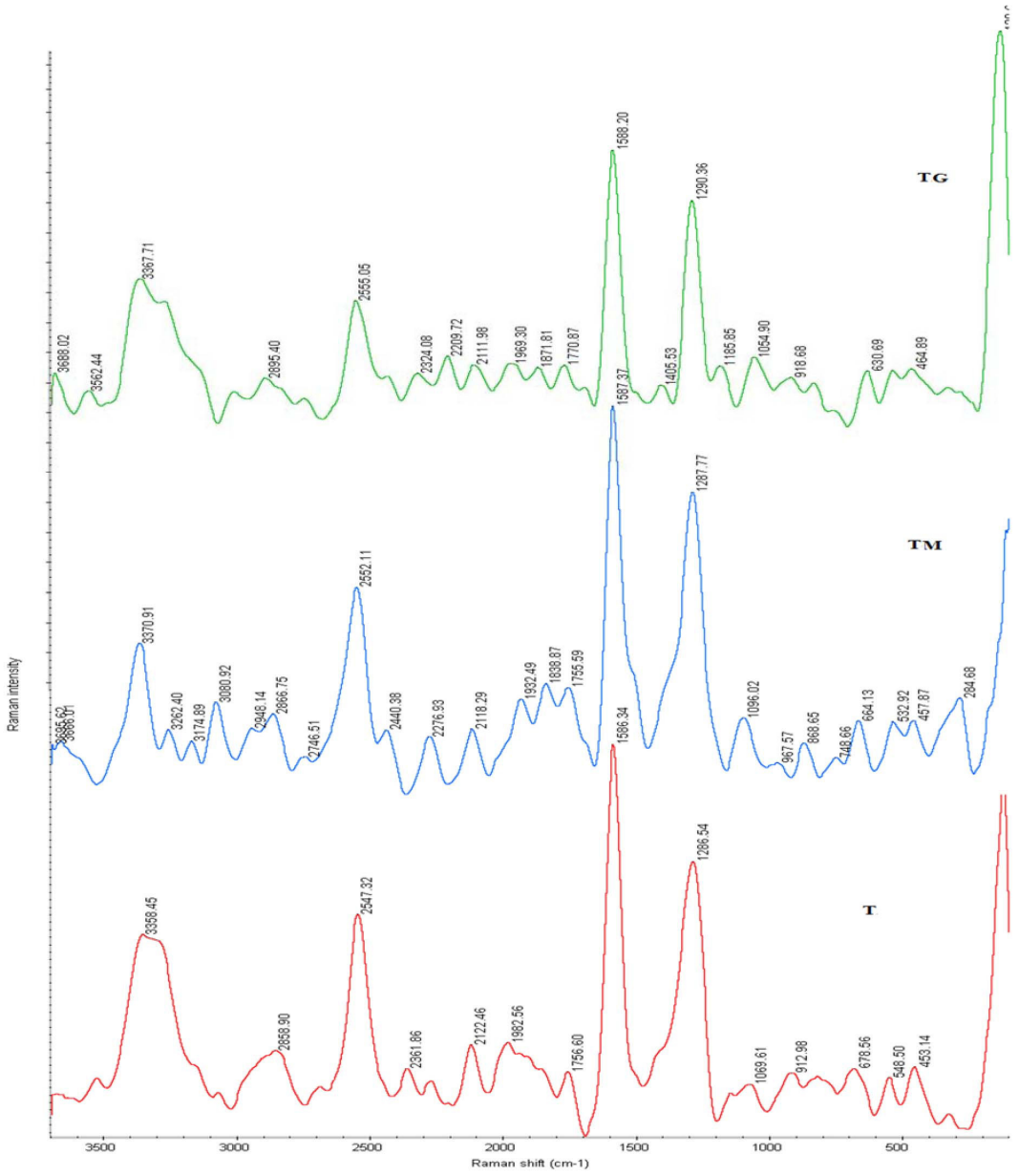

Fig. 3. Raman spectra of powder samples of Ti-NPs.

FE-SEM and EDXS

FE-SEM was used to characterize the surface morphology of Ti-NPs (Fig. 4). The average particle sizes of samples T, TM, and TG were 23, 24, and 22 nm, respectively. The results indicated the generation of fine-grained, hybrid compounds with clear porous surface structures in the hybrid compounds. The chemical compositions of the samples were determined using EDXS. Fig. 4 shows the incorporation of carbon into the TiO_2 lattices. The FE-SEM images showed that TG had a reasonable particle size distribution and no aggregation compared with other samples, which agrees with the literature [36-37]. As observed in the EDXS tables, the spectral series of the elements in this compound was type K_α, indicating that an electron has left the K layer and has been replaced by an electron from the L layer.

XRD

The crystal structure and phase of Ti-NPs were determined using XRD. As observed, the major phase of all samples was anatase. Fig. 5 shows the XRD patterns of the catalysts, and more details are found in Table 4 [38-39].

BET Surface Area Analysis

BET was used to determine the specific surface areas of Ti-NPs. As shown in Table 5, the specific surface area has increased by adding Ti-NPs to the carbonaceous structure. Oxide groups have formed between the carbon layers of GO and nanotubes due to calcination, and the interlayer distance increases, which then increases the specific surface [38-39].

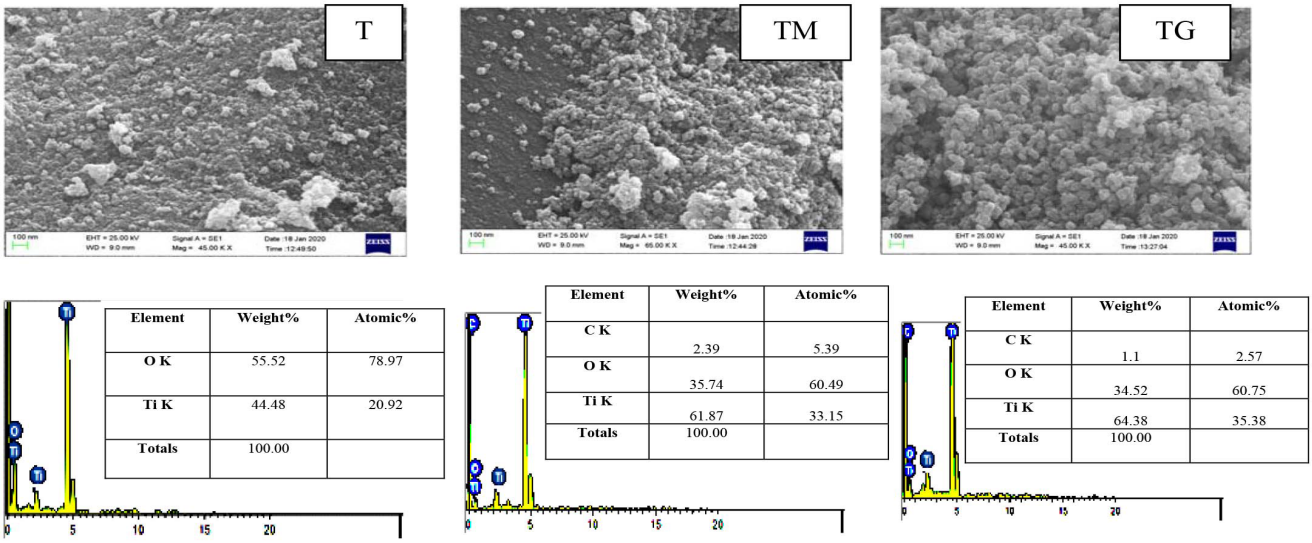

Element	Weight%	Atomic%
O K	55.52	78.97
Ti K	44.48	20.92
Totals	100.00	

Element	Weight%	Atomic%
C K	2.39	5.39
O K	35.74	60.49
Ti K	61.87	33.15
Totals	100.00	

Element	Weight%	Atomic%
C K	1.1	2.57
O K	34.52	60.75
Ti K	64.38	35.38
Totals	100.00	

Fig. 4 FE-SEM & EDXS analyses of Ti-NPs: the EDXS was determined under full scale 100 cts Cursor: 0.000 (keV).

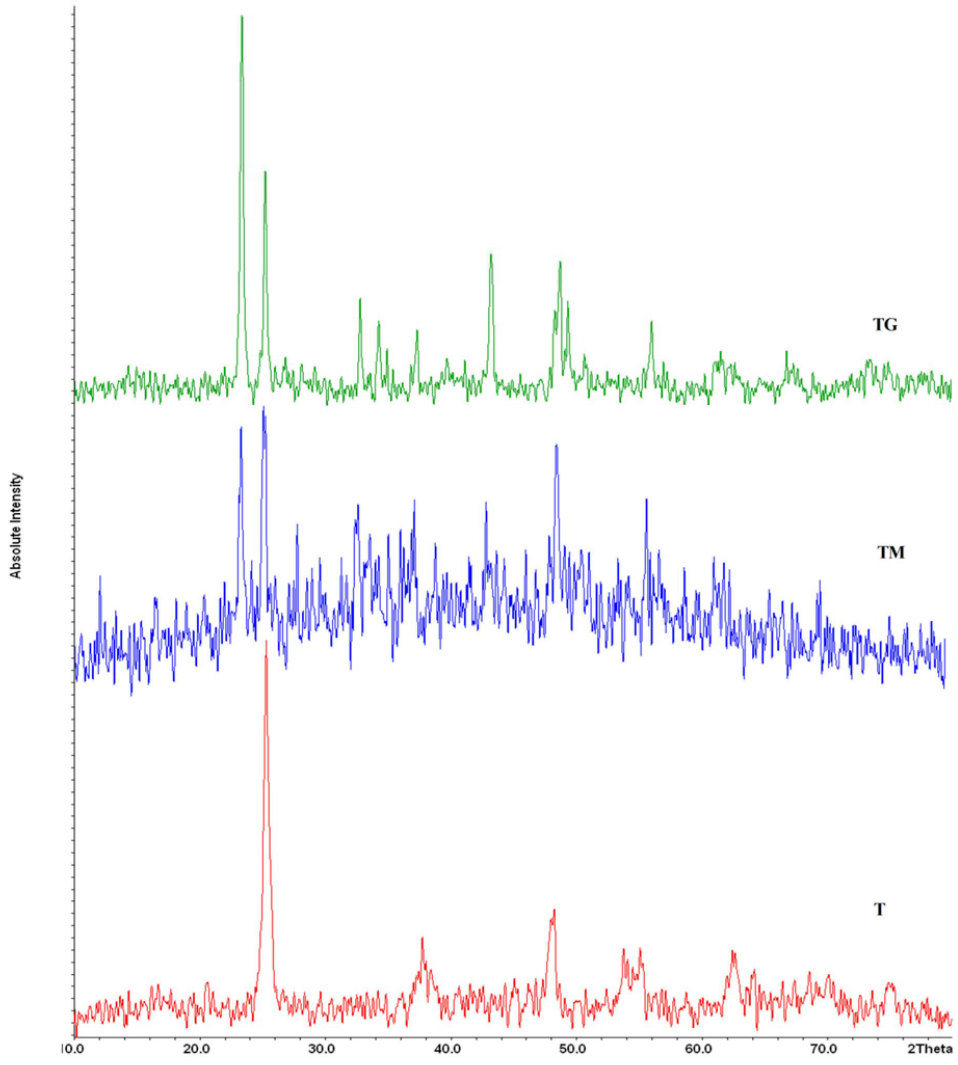

Fig. 5 XRD patterns of Ti-NPs.

Table 4 XRD Analysis

	T	TM	TG
	Observed peak (hkl)*	Standard peak	
*XRD Major peak, 2θ°	**TiO_2**: 25.26, (101), 25.2 **TiO_4**: 25.7, (112), 25 32.10, (112) 36.51, (130) 49.07, (204)	**TiO_2**: 25.30, (101), 25.2 **$Ti_{1.23}O_{2.13}$**: 25.6,(112), 25 32.10, (112) 36.4, (130) 49.20, (204) **C**: 10.81,(111), 11	**TiO_2**: 25.22, (101), 25.2 **$Ti_{1.25}O_{2.15}$**: 25.2, (112), 25 32.10, (112) 36.01, (130) 49.35,(222) **C**: 26.22,(002), 25
Crystal phase	TiO_2 (anatase) + TiO_4	TiO_2 (anatase) + $Ti_{1.23}O_{2.13}$	TiO_2 (anatase) + $Ti_{1.25}O_{2.15}$
Crystal size Scherrer equation, nm	25	28	24

* The Miller Indices (hkl) are a set of numbers to quantify the intercepts and thus may be used to identify the plane or surface uniquely.

Table 5 BET Surface Area Analysis.

Sample	Specific Surface Area, (m^2/g)
T	108
TM	192
TG	215

In general, the kinetic behavior of absorption of Ti-Nps (Fig. 6) can be expressed by the Langmuir-Hinshelwood equation (Equation 2).

$$r = -\frac{dc}{dt} = \frac{k_r k_{ad} c}{1 + k_{ad} c} \quad (2)$$

where k_r and k_{ad} represent the reaction rate and equilibrium constants of adsorption, respectively. As the diagram shows, the adsorption of TG was higher than that of T due to the increased surface area. Therefore, the above relationship is linear. The processing results and the equations corresponding to the first-order kinetics plot were used to calculate the rate constant in the adsorption process and confirm its first-order nature. The results indicated a high convergence coefficient.

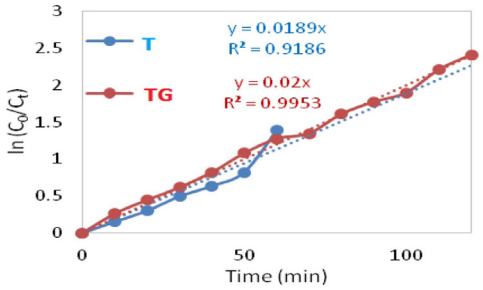

Fig. 6 Kinetics of the adsorption process.

HR-TEM

The nanostructure of the samples was studied by HR-TEM. According to the results (Fig. 7), the average T, TM, and TG particle sizes were 26, 27, and 27 nm, respectively. HR-TEM also confirmed the good dispersion of all samples with no aggregation [38-39].

DRS

The band gap energies (EBG) of Ti-Nps were determined using Equation 3. Fig. 8 and Table 6 show the results. The E_{BG} values of TiO_2 have decreased by adding carbonaceous substrate, causing increased activity of Ti-Nps [40-41].

$$E_{BG} = \frac{1240}{\lambda} \quad (3)$$

Thermogravimetric Analysis (TGA)

Fig. 9 shows the TGA curves of the synthesized Ti-NPs. The thermal stability of Ti-NPs was studied under an N_2 atmosphere. The temperature effect on weight loss can be investigated for the entire heating profile. The sample weight and temperature were about 15 mg and 50-600°C, respectively. A 100 ml ×$min.^{-1}$ flow of highly pure N_2 was used at a 10°C×$min.^{-1}$ heating rate. The TGA curves revealed no peaks corresponding to weight loss on increasing the temperature, which is due to the thermal stability of the samples. The curves also showed the complete separation of the excess solvents and volatile compounds during calcination. Therefore, the samples remain stable during the bottle test.

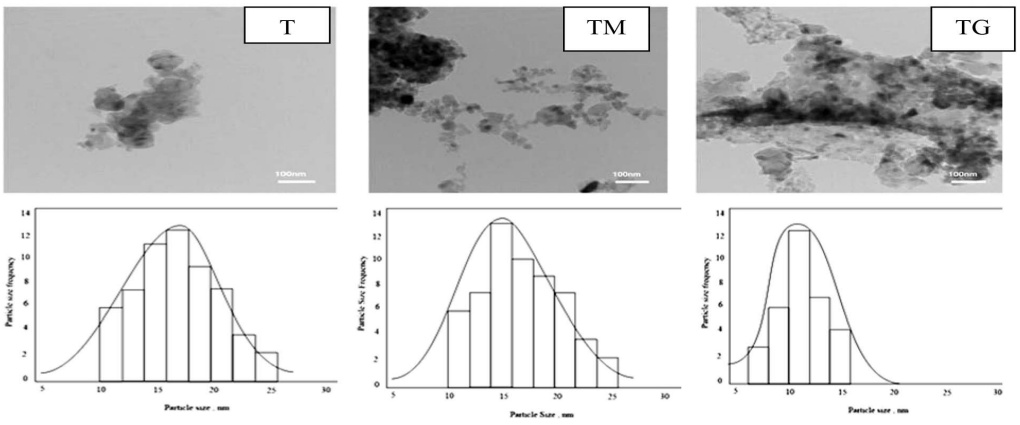

Fig. 7 HR-TEM of Ti-NPs; with normal particle size distribution of their histogram.

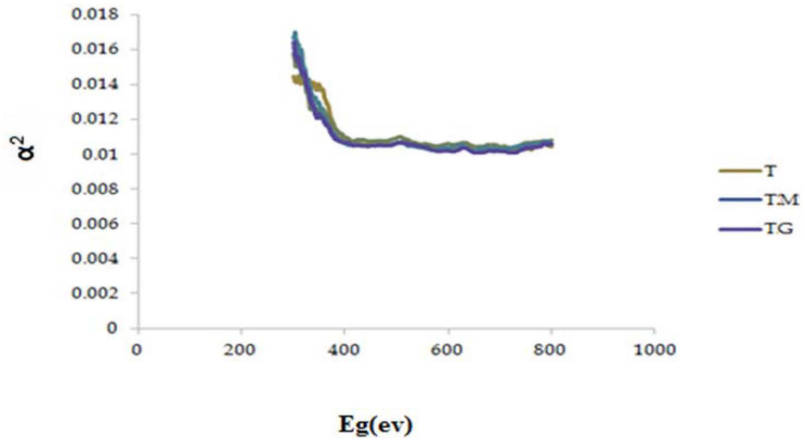

Fig. 8 DRS of Ti-NPs.

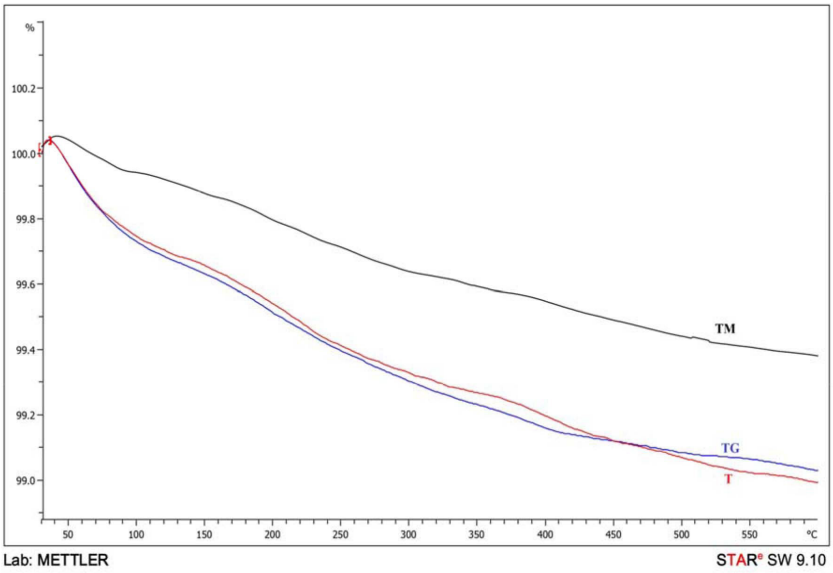

Fig. 9 TGA of Ti-NPs (at N_2 atmosphere).

Table 6 E_{BG} of Ti-NPs.

	T	TM	TG
E_{BG}, eV	3.33	2.20	2.09
λ, nm	372	563	593

Statistical Analysis of the Demulsification Experiment

Initially, the demulsification efficiency of different Ti-NPs was evaluated using 50 and 100 ppm dosages, 60 and 120 min, settling times, and 50 and 70°C temperatures to select the optimal sample for experimental design. Nano TiO_2 hybridized with (GO) could increase the water removal efficiency compared with the other samples and the blank. According to Fig. 10 and Table 7, the demulsification efficiency was as follows: TG > TM > T > Blank.

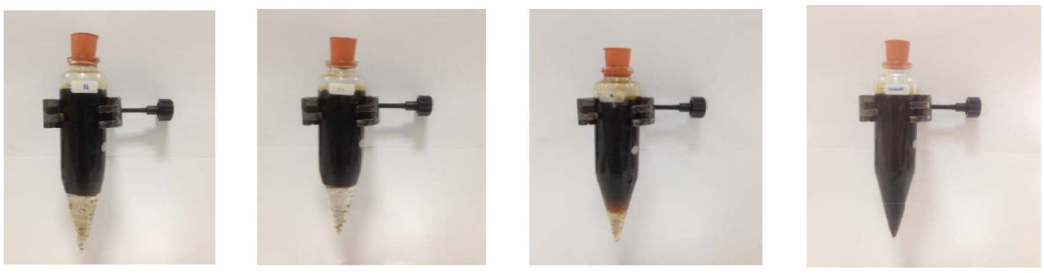

Fig. 10 Demulsification efficiency at concentration, time, and temperature of 100 ppm, 120 min. and 70°C, respectively (entry 8, Table 5); TG > TM > T > Blank.

Table 7 Screening of efficiency of Ti-NPs under different conditions for water separation from crude oil.

				Water separation, %			
	Temperature, °C	Concentration, ppm	Time, min.	Blank	T	TM	TG
1	50	50	60	0	15	30	45
2	50	100	60	0	33	53	67
3	70	50	60	0	30	46	53
4	70	100	60	0	55	67	75
5	50	50	120	0	35	46	60
6	50	100	120	0	46	70	80
7	70	50	120	0	53	65	75
8	70	100	120	0	60	80	95

Based on the screening test results, the superior performance of the sample containing GO was expected. GO can break the layer between the crude oil and water and thus decrease the surface tension due to its biocompatibility, solubility, and structural active sites. GO is made considerably hydrophilic by the functional groups containing oxygen. Upon the addition of GO to the TiO_2 matrix, the hydrophilicity and demulsification properties will improve. In addition, the self-assembly of TG at the W/O interface shows its capability of destroying the rigid interfacial film by adsorption or displacement of the asphaltenes *via* π-π interaction, which helps separation [17-18, 21]. TM was modified by adding –COOH through covalent functionalization to improve its demulsification efficiency [17-18, 21]. After selecting a high-performance sample (TG), a combination of the RSM method and CCD approach was used to study the impact of the experimental parameters on the final nanoparticle surface area by a set of 20 experiments. Temperature, demulsifier dosage, and time-independent variables were investigated at three levels, coded –1, 0, and +1, where α was 1.633. The water separation percentage from crude oil (R%) was chosen as the system response (Y). Table 8 shows the coded values of the variables. Table 9 shows the DOE results in the bottle tests.

Table 8 Coded and un-coded values of experimental factors.

	Coded values				
Variable	1.633	1	0	-1	-1.633
X1 (Temperature, °C)	89.495	80	65	50	40.505
X2 (Concentration, ppm)	181.65	150	100	50	18.35
X3 (Time, min.)	292.222	75	157.5	240	22.778

Table 9 Results of experiments based on RSM-CCD.

				Water separation, %
Run No.	Temperature	Concentration	Time	TG
1	1	–1	1	67
2	–1	–1	–1	47
3	1	–1	–1	60
4	–1	–1	1	53
5	1	1	1	100
6	–1	1	1	93
7	–1	1	–1	73
8	1	1	–1	93
9	0	0	0	97
10	0	0	0	97
11	0	0	0	95
12	0	0	0	95
13	0	0	0	97
14	0	0	0	100
15	1.633	0	0	95
16	0	1.633	0	95
17	0	0	1.633	93
18	–1.633	0	0	60
19	0	–1.633	0	47
20	0	0	–1.633	53

Statistical testing of the TG model was confirmed by the coded coefficient and the ANOVA. Tables 10 and 11 show a summary of the corresponding data.

The significance level of the model was evaluated using the F and P-values. The majority of the P-values were below 0.05, indicating the statistical importance of the model terms for TG. Water removal by TG is a function of concentration, temperature, and time and is given by the regression equation (Equation 4) obtained from the ANOVA.

TG = 96.61 + 8.34 Temp. + 15.78 Concen. + 7.90 Time – 6.72 Temp.×Temp. – 9.16 Concen.×Concen. -8.41 Time×Time + 0.00 Temp.×Concen. – 1.50 Temp.×Time + 1.75 Concen.×Time (4)

The significant terms in the model developed for predicting the demulsification efficiency of TG, that is, temperature, concentration, and time had positive and valuable impacts, unlike the squared parameters. Due to the lack of 2-way interaction of (temp. concen.), it can be eliminated. The P-values were higher than 0.05, indicating the significance of the model terms for 2-way interaction TG. Therefore, Equation 5 is rewritten as follows:

TG = 96.61 + 8.34 Temp. + 15.78 Concen. + 7.90 Time – 6.72 Temp.×Temp. – 9.16 Concen. ×Concen.- 8.41 Time×Time – 1.50 Temp.×Time + 1.75 Concen. ×Time (5)

The desired R^2 value is close to unity. The full factorial DOE has been used to investigate all factors and level combinations. The DOE can determine the significance of all the interactions, including those not considered in experimenting with one factor at a time (Table 12).

Table 13 shows the optimal conditions achieved by statistical optimization with maximum water removal based on the DOE and bottle test results.

Table 10 The coded coefficient of demulsification efficiency of TG.

	Coef.	SE Coef.	T-value	P-value	VIF
Constant	96.61	2.29	0.000	42.15	2.29
X1 (Temperature, °C)	8.34	1.53	5.43	0.000	1.00
X2 (Concentration)	15.78	1.53	10.29	0.000	1.00
X3 (Time, min.)	7.90	1.53	5.15	0.001	1.00
$X1^2$	–6.72	1.54	–4.36	0.001	1.01
$X2^2$	–9.16	1.54	–5.94	0.002	1.01
$X3^2$	–8.41	1.54	–5.46	0.000	1.01
X1X2	0.00	1.98	0.00	1.000	1.00
X1X3	–1.50	1.98	–0.76	0.468	1.00
X2X3	1.75	1.98	0.88	0.400	1.00

Table 11 The ANOVA calculation on the demulsification efficiency of TG.

	DF	Adj-SS	Adj-MS	F-value	P-value
Model	10	796.92	796.92	16.40	0.000
Blocks	1	16.14	16.14	0.33	0.752
Linear	3	1970.05	1970.05	40.54	0.000
X1 (Temperature, °C)	1	946.18	946.18	19.47	0.000
X2 (Concentration)	1	3815.41	3815.41	78.51	0.000
X3 (Time, min.)	1	1148.57	1148.57	23.63	0.001
$X1^2$	1	527.05	527.05	10.84	0.002
$X2^2$	1	1012.23	1012.23	20.83	0.000
$X3^2$	1	768.80	768.80	15.82	0.000
X1X2	1	6.12	6.12	0.13	1.000
X1X3	1	3.12	3.12	0.06	0.468
X2X3	1	6.12	6.12	0.13	0.400

Table 12 The R2 value of demulsification efficiency of TG.

	R^2	R^2 (adj)
TG	96.34%	92.28%

Table 13 Optimization of demulsification efficiency of TG. Predicted and experimental results.

Variable	Setting	Model Predicted	Experimental
Temperature, °C	65	95%	~100%
Concentration, ppm	75		
Time, min.	120		

Fig. 11 shows the 2-D diagrams of the variations in the corresponding factors. The variations in the concentration, temperature, and time ranges were modified to lower levels necessary for the water removal compared with those of previously reported high-efficiency demulsifiers. The darker areas in the contour diagrams indicate the most water removal. The (time×concentration) diagram has been determined based on the 65 °C constant temperature and the maximum water removal at the time and concentration of about 150 min. and 110 ppm, respectively. The remaining diagrams may be interpreted similarly.

Based on the performance of TG *vs*. each of the three factors shown in Fig. 12 (a-c), the response behavior can be followed by keeping one factor fixed at the center point (Xi=0) while varying the other two factors near the center point. Consequently, the final results can provide the best responses under optimal conditions. The impacts of optimal and low concentrations on TG performance may be thoroughly observed in Figs. 13 and 14. As observed, the positive effects of temperature and concentration on the yield can be detected simultaneously. Moreover, the optimal area in this work was appropriately chosen. Although these plots showed no absolute maximum around the center point, the optimal conditions have been selected, and maximum demulsification efficiency has been achieved.

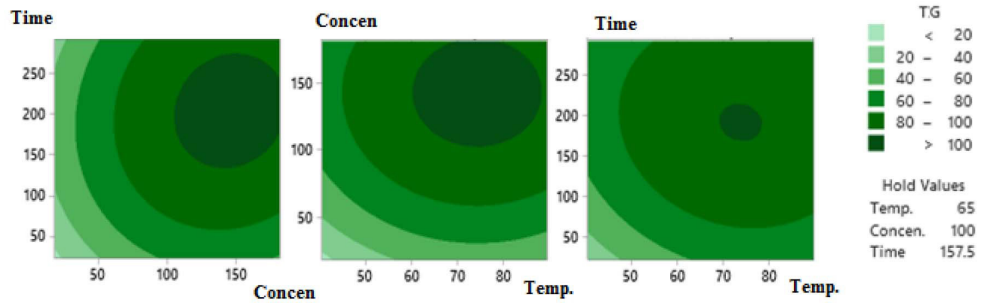

Fig. 11 Contour plots of demulsification efficiency of TG.

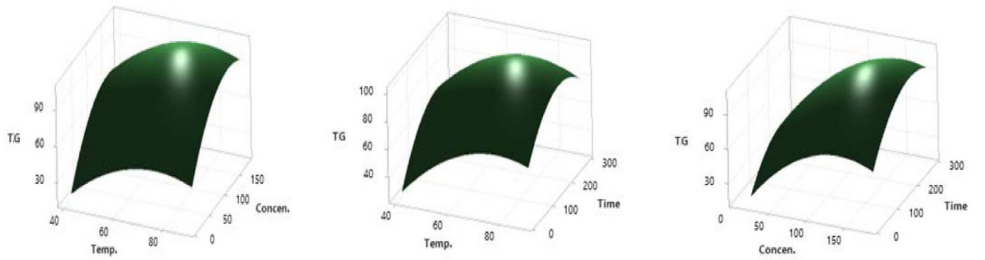

(a) – TG *vs*. Concen., Temp. – Hold Values; Time 157.5 min.

(b) – TG *vs*. Time, Temp. – Hold Values; Concen. 100 ppm.

(c) – TG *vs*. Time, Concen. – Hold Values; Temp. 65°C.

Fig. 12 Surface plots of demulsification efficiency of TG.

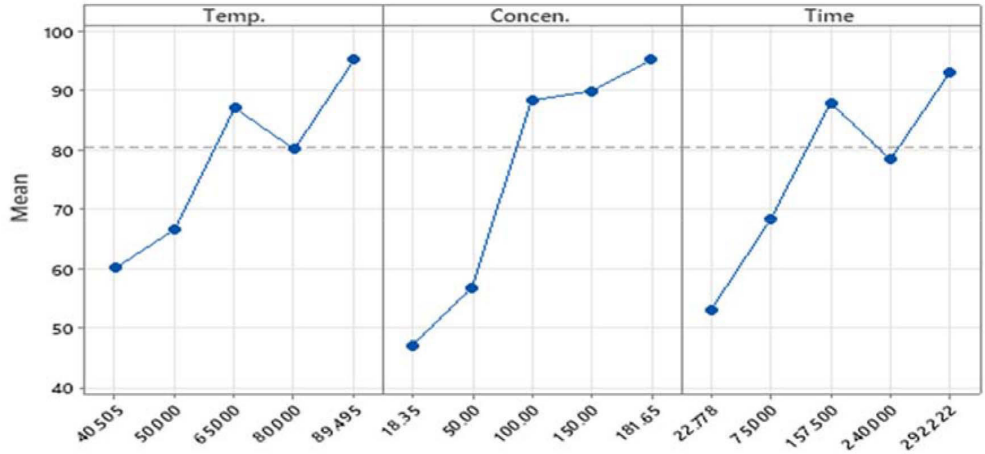

Fig. 13 Main effects plots of demulsification efficiency of TG.

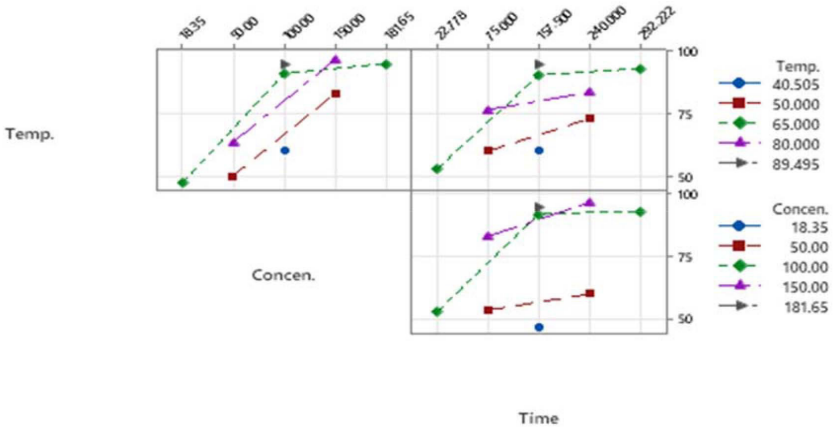

Fig. 14 Interaction plots of demulsification efficiency of TG.

The results of this study have been compared with those of previous reports (Table 14). The composite performed better when prepared under optimal conditions than compounds with similar structures [18, 20-24] in the presence of mineral dioxide and carbon-containing compounds [18, 20-24]. The results of demulsification activity indicated the outstanding efficiency of Ti-NPs compared with the values reported at lower temperatures, concentrations, and optimal times. Furthermore, the removed water was non-oily and clear. Separation percentages revealed that the specific surface area increased by substrating Ti-NPs on the carbonaceous structure, causing improved demulsification. The results indicated that hydrophobic substrates favored demulsification.

Table 14 Comparison of the demulsification efficiency of Ti-NPs and different nanoparticles.

Demulsifiers	Emulsion type	Demulsification Temperature, °C	Concentration of demulsifier, ppm	Demulsification time, min.	Demulsification Efficiency (DE)	Refs.
RGO/TiO_2	oily waste water	Ambient temperature	500	30	80%	[10]
Magnetically responsive multi-walled carbon nanotubes (M-MWCNTs)	crude oil	Ambient temperature to 60	400	120	95.5%	[12]
Silica nanoparticles	heavy crude oil	75	30-60-90	180-1440	Up to 53%	[15]
κCaGO	heavy crude oil	Ambient temperature	1000-5000-10000	120	70%	[18]
Nano titanium dioxide	crude oil	60	30	720	22-56%	[19]
CNTs/TiO_2	oily waste water	Ambient temperature	400	30	89.7%	[20]
CT/Ti-NPs	crude oil	65	100	100	~100%	[25]
Ti-NPs (TG)	crude oil	65	70	120	~100%	This work

Conclusions

Various nano TiO_2-based carbonaceous demulsifiers have been synthesized by the sol-gel method and used as chemical demulsifiers of W/O emulsions. The effects of changing the surface area of the nanocomposite and particle size, synthesized on oil as chemical demulsifiers, were studied. The addition of carbonaceous compounds improved the performance of TiO_2 nanoparticles. The results revealed that the surface area increased the incorporation of a carbonaceous substrate (graphene oxide). Remarkably higher demulsification efficiency was shown by TG nanoparticles compared with the previously reported demulsifiers. Ti-NPs based on a carbonaceous substrate (graphene oxide) showed considerably higher demulsification efficiency than the other samples under optimal conditions. In addition, sample TG can be introduced as a good example of enhanced nano demulsification compared with similar demulsifiers reported in dosage, separation time, and temperature.

References

1. Wang, D., Yang, D., Huang, C., Huang, Y., Yang, D., Zhang, H., & Zeng, H. (2021). Stabilization mechanism and chemical demulsification of water-in-oil and oil-in-water emulsions in petroleum industry: A review, Fuel, 286, 119390, doi:10.1016/j.fuel.2020.119390.
2. Chen, Z., Peng, J., Ge, L., & Xu, Z. (2015). Demulsifying water-in-oil emulsion by ethyl cellulose demulsifiers studied using focused beam reflectance measurement, Chemical Engineering Science, 130, 254-263, doi:10.1016/j.ces.2015.03.014.
3. Kokal, S. (2005). Crude oil emulsions: A State-of-the-Art Review, SPE Production & Facilities, 20, 1, 5-13, doi:10.2118/77497-PA.
4. Silva, F. L. M. C., Tavares, F. W., & Cardoso, M. J. E.

M. (2013). Thermodynamic stability of water-in-oil emulsions, Brazilian Journal of Petroleum and Gas, 7, 1, 1-13, doi:10.5419/bjpg2013-0001.
5. Zhang, Z., Wang, Z., Zhang, H., Wang, Q., Tang, Y., Qu, Q., & Yan, X. (2023). An ionic liquid demulsifier with double cationic centers and multiple hydrophobic chains, Journal of Molecular Liquids, 374, 121265, doi:10.1016/j.molliq.2023.121265.
6. Azizi, N., & Bashipour, F. (2022). Demulsification of water-in-oil emulsions applying Fe_3O_4 magnetic nanoparticles for demulsifier modification: Experimental optimization *via* response surface methodology, Journal of Petroleum Science and Engineering, 216, 110806, doi:10.1016/j.petrol.2022.110806.
7. Sadighian, H., Ahmadi, E., & Mohamadnia, Z. (2023). Application of imidazolium based ionic liquids grafted on microcrystalline cellulose as demulsifiers for water in crude oil (W/O) emulsions, Carbohydrate Polymer, 302, 120406, doi:10.1016/j.carbpol.2022.120406.
8. Dhandhi, Y., Prakash, O., Naiya, T. K., & Guria, C. (2022). Statistical design and process optimization for using chemical demulsifiers for the dehydration of the crude oil, Journal of Petroleum Science and Engineering, 217, 110876, doi: 10.1016/j.petrol.2022.110876.
9. Hjartnes, T. N., Sørland, G. H., Simon, S., & Sjöblom, J. (2019). Demulsification of crude oil emulsions tracked by pulsed field gradient (PFG) nuclear magnetic resonance (NMR). Part I: Chemical demulsification, Industrial & Engineering Chemistry Research, 58: 6, 2310-2323, doi: 10.1021/acs.iecr.8b05165.
10. Shubair, A., Al-Salih, H., Sabouni, R., Gomaa, H., Hassanin, S., Salem, S., & Zaka, A. (2021). Photocatalytic demulsification of oil/water emulsions containing nonionic surfactant, Environmental Science and Pollution Research (ESPR), 28, 13124-13132, doi:10.1007/s11356-020-11541-1.
11. Ye, F., Wang, Z., Mi, Y., Kuang, J., Jiang, X., Huang, Z., & Zhang, Z. (2020). Preparation of reduced graphene oxide/ titanium dioxide composite materials and its application in the treatment of oily wastewater, Colloids and Surfaces A: Physicochemical and Engineering Aspects, 586, 124251, doi: 10.1016/j.colsurfa.2019.124251.
12. Fong, K. K., Tan, I. S., Foo, H. C. Y., Lam, M. K., Tiong, A. C. Y., & Lim, S. (2021). Optimization and evaluation of reduced graphene oxide hydrogel composite as a demulsifier for heavy crude oil-in-water emulsion, Chinese Journal of Chemical Engineering, 33, 297-305, doi:10.1016/j.cjche.2020.08.027.
13. Chang, S. M., Hou, C. Y., Lo, P. H., & Chang, C. T. (2009). Preparation of phosphated Zr-doped TiO_2 exhibiting high photocatalytic activity through calcination of ligand-capped nanocrystals, Applied Catalysis B: Environmental, 90, 233-241, doi:10.1016/j.apcatb.2009.03.009.
14. Seetharaman, A., & Dhanuskodi, S. (2014). Micro-structural, linear and nonlinear optical properties of titania nanoparticles. Spectrochimica Acta Part A, 127, 543-549, doi:10.1016/j.saa.2014.02.164.
15. Hassan, S. A., Abdalla, B. K., & Mustafa, M. A. (2019). Addition of silica nanoparticles for the enhancement of crude oil demulsification process, Petroleum Science and Technology, 37, 1603-1611, doi:10.1080/10916466.2019.1602634.
16. Xue, Z., Cao, Y., Liu, N., Feng, L., & Jiang, L. (2014). Special wettable materials for oil/water separation, Journal of Materials Chemistry A, 2, 2445-2460, doi:10.1039/C3TA13397D.
17. Xu, H., Jia, W., Ren, S., & Wang, J. (2019). Magnetically responsive multi-wall carbon nanotubes as recyclable demulsifier for oil removal from crude oil-in-water emulsion with different pH levels, Carbon, 145, 229-239, doi:10.1016/j.carbon.2019.01.024.
18. Ye, F., Wang, Z., Mi, Y., Kuang, J., Jiang, X., Huang, Z., & Zhang, Z. (2020). Preparation of reduced graphene oxide/ titanium dioxide composite materials and its application in the treatment of oily wastewater, Colloids and Surfaces A: Physicochemical and Engineering Aspects, 586, 124251, doi: 10.1016/j.colsurfa.2019.124251.
19. Nikkhah, M., Tohidian, T., Rahimpour, M. R., & Jahanmiri, A. (2015). Efficient demulsification of water-in-oil emulsion by a novel nano-titania modified chemical demulsifier, Chemical Engineering Research and Design, 94, 164-172, doi: 10.1016/j.cherd.2014.07.021.
20. Jiang, X., Ye, F., Zheng, L., Mi, Y., Zhang, Z., Yuan, H., & Luo, Y. (2020). Multi-walled carbon nanotubes grafted by polyvinyl alcohol and its demulsification performance in oily wastewater, Chemistry Select, 5: 26, 7895-7900, doi:10.1002/slct.202001792.
21. Mombeshora, E. T., Simoyi, R., Nyamori, V. O., & Ndungu, P. G. (2015). Multi-walled carbon nanotube-titania nanocomposites: Understanding nano-structural parameters and functionality in dye-sensitized solar cells, Journal of Chemical Education, 68, 153-164, doi:10.17159/0379-4350/2015/V68A22.
22. Feinle, A., Elsaesser, M. S., & Huesing, N. (2016). Sol-gel synthesis of monolithic materials with hierarchical porosity, Chemical Society Reviews, 45, 3377-3399, doi: 10.1039/C5CS00710K.
23. Owens, G. J., Singh, R. K., Foroutan, F., Alqaysi, M., Han, C. M., Mahapatra, C., & Knowles, J. C. (2016). Sol-gel based materials for biomedical applications, Progress in Materials Science, 77, 1-79, doi:10.1016/j.pmatsci.2015.12.001.
24. Mäkelä, M. (2017). Experimental design and response surface methodology in energy applications: A tutorial review, Energy Conversion and Management, 151, 630-640, doi:10.1016/j.enconman.2017.09.021.
25. Bigdeli, T., Shekarriz, M., Mehdizadeh, A., & Ahmadi, A. N. (2022). Eco-friendly and efficient demulsification by chitosan biopolymer modified with titanium dioxide nanohybrid on carbonaceous substrates in (W/O) emulsions of crude oil, Journal of Sol-Gel Science and Technology, doi;10.1007/s10971-022-05907-9.
26. Zhao, G., Tian, Q., Liu, Q., & Han, G. (2005). Effects of HPC on the microstructure and hydrophilisity of sol-gel-derived TiO_2 films, Surface and Coatings Technology, 198, 55-58, doi: 10.1016/j.surfcoat.2004.10.064.
27. Razi, M., Rahimpour, M. R., Jahanmiri, A., & Azad, F. (2011) Effect of a different formulation of demulsifiers on the efficiency of chemical demulsification of heavy

crude oil, Journal of Chemical & Engineering Data, 56, 2936-2945, doi: 10.1021/je2001733.
28. Razi, M., Rahimpour, M. R., Jahanmiri, A., & Azad, F. (2011). Structural characterization of the sol-gel oxide powders from the ZnO-TiO_2-SiO_2 system, Superlattices and Microstructures, 42, 314-321, doi: 10.1016/j.spmi.2007.04.004.
29. Wang, C., Xu, B. Q., Wang, X., & Zhao, J. (2005). Preparation and photocatalytic activity of ZnO/TiO_2/SnO_2 mixture, Journal of Solid State Chemistry, 178, 3500-3506, doi:10.1016/j.jssc.2005.09.005.
30. Liao, M. H., Hsu, C. H., & Chen, D. H. (2006). Preparation and properties of amorphous titania-coated zinc oxide nanoparticles, Journal of Solid State Chemistry, 179, 2020-2026, doi: 10.1016/j.jssc.2006.03.042.
31. Karthik, K., Pandian, S. K., & Jaya, N. V. (2010). Effect of nickel doping on structural, optical and electrical properties of TiO_2 nanoparticles by sol-gel method, Applied Surface Science, 256, 6829-6833, doi:10.1016/j.apsusc.2010.04.096.
32. Choi, H. C., Jung, Y. M., & Kim, S. B. (2005). Size effects in the Raman spectra of TiO_2 nanoparticles, Vibrational Spectroscopy, 37, 33-38, doi: 10.1016/j.vibspec.2004.05.006.
33. Truijen, I., Haeldermans, I., Van Bael, M. K., Van den Rul, H., D'Haen, J., Mullens, J., & Goossens, V. (2007). Influence of synthesis parameters on morphology and phase composition of porous titania layers prepared *via* water based chemical solution deposition, Journal of the European Ceramic Society, 27, 4537-4546, doi:10.1016/j.jeurceramsoc.2007.02.200.
34. Miao, L., Tanemura, S., Toh, S., Kaneko, K., & Tanemura, M. (2004). Fabrication, characterization and Raman study of anatase-TiO_2 nanorods by a heating-sol-gel template process, Journal of Crystal Growth, 264, 246-252, doi:10.1016/j.jcrysgro.2003.12.027.
35. Ren, D., Bei, Z., Shen, J., Cui, X., Yang, X., & Zhang, Z. (2005). The structure change and the superhydrophilicity of the Sb-doped titanium dioxide thin film, Journal of Sol-Gel Science and Technology, 34, 123-126, doi:10.1007/s10971-005-1330-4.
36. Xinshu, N. I. U., Sujuan, L. I., Huihui, C. H. U., & Jianguo, Z. H. O. U. (2011). Preparation, characterization of Y3+-doped TiO_2 nanoparticles and their photocatalytic activities foe methyl orange degradation, Journal of Rare Earths, 29, 225-229, doi:10.1016/S1002-0721(10)60435-8.
37. Chen, C., Wang, Z., Ruan, S., Zou, B., Zhao, M., & Wu, F. (2008). Photocatalytic degradation of CI Acid orange 52 in the presence of Zn-doped TiO_2 prepared by a stearic acid gel method, Dyes and Pigments, 77, 204-209, doi:10.1016/j.dyepig.2007.05.003.
38. Akpan, U. G., & Hameed, B. H. (2010). The advancements in sol-gel method of doped-TiO_2 photocatalysts, Applied Catalysis A: General, 375, 1-11, doi:10.1016/j.apcata.2009.12.02.3
39. Li, Y., Peng, S., Jiang, F., Lu, G., & Li, S. (2007). Effect of doping TiO_2 with alkaline-earthmetal ions on its photocata-lytic activity, Journal of the Serbian Chemical Society - JSCS, 72, 393-402, doi:10.2298/JSC0704393L.
40. Sharma, M., Kumar, S., & Pandey, O. P. (2010). Study of energy transfer from capping agents to intrinsic vacancies/defects in passivated ZnS nanoparticles, Journal of Nanoparticle Research, 12, 2655-2666, doi: 10.1007/s11051-009-9844-2.
41. Zachariah, A., Baiju, K. V., Shukla, S., Deepa, K. S., James, J., & Warrier, K. G. K. (2008). Synergistic effect in photocatalysis as observed for mixed-phase nanocrystalline titania processed *via* sol−gel solvent mixing and calcination, The Journal of Physical Chemistry C, 112, 30, 11345-11356, doi: 10.1021/jp712174y.